

Article

Theoretical Investigations of the Structural, Dynamical, Electronic, Magnetic, and Thermoelectric Properties of CoMRhSi ($M = \text{Cr}, \text{Mn}$) Quaternary Heusler Alloys

Abdullah Hzzazi ^{1,2}, Hind Alqurashi ^{3,4}, Eesha Andharia ^{1,3,*}, Bothina Hamad ^{1,5,*} and M. O. Manasreh ⁶

¹ Department of Physics, University of Arkansas, Fayetteville, AR 72701, USA; ahzzazi@uark.edu or abdullahhzzazi@gmail.com

² Basic Sciences Department, King Saud Bin Abdulaziz University for Health Sciences, Riyadh 14611, Saudi Arabia

³ Materials Science and Engineering, University of Arkansas, Fayetteville, AR 72701, USA; halquras@uark.edu

⁴ Physics Department, College of Science, Al-Baha University, Alaqiq 65779, Saudi Arabia

⁵ Physics Department, The University of Jordan, Amman 11942, Jordan

⁶ Department of Electrical Engineering, University of Arkansas, Fayetteville, AR 72701, USA; manasreh@uark.edu

* Correspondence: esandhar@uark.edu (E.A.); bothinah@uark.edu (B.H.)

Abstract: The structural, dynamical, electrical, magnetic, and thermoelectric properties of CoMRhSi ($M = \text{Cr}, \text{Mn}$) quaternary Heusler alloys (QHAs) were investigated using density functional theory (DFT). The Y-type-II crystal structure was found to be the most stable configuration for these QHAs. Both CoCrRhSi and CoMnRhSi alloys possess a half-metallic behavior with a 100% spin-polarization as the majority spin channel is metallic. On the other hand, the minority spin channel is semiconducting with narrow indirect band gaps of 0.54 eV and 0.57 eV, respectively, along the $\Gamma - X$ high symmetry line. In addition, both CoCrRhSi and CoMnRhSi alloys possess a ferromagnetic structure with total magnetic moments of 4 μ_B , and 5 μ_B , respectively, which are prominent for spintronics applications. The thermoelectric properties of the subject QHAs were calculated by using Boltzmann transport theory within the constant relaxation time approximation. The lattice thermal conductivities were also evaluated by Slack's equation. The predicted values of the figure-of-merit (ZT) for CoCrRhSi and CoMnRhSi were found to be 0.84 and 2.04 at 800 K, respectively, making them ideal candidates for thermoelectric applications.

Keywords: ab initio investigations; quaternary Heusler; transport coefficients; Slack's equation; ferromagnetic; half-metallic



Citation: Hzzazi, A.; Alqurashi, H.; Andharia, E.; Hamad, B.; Manasreh, M.O. Theoretical Investigations of the Structural, Dynamical, Electronic, Magnetic, and Thermoelectric Properties of CoMRhSi ($M = \text{Cr}, \text{Mn}$) Quaternary Heusler Alloys. *Crystals* **2024**, *14*, 33. <https://doi.org/10.3390/cryst14010033>

Academic Editors: Dmitri Donetski, Thomas M. Klapötke and Raphaël P. Hermann

Received: 8 November 2023

Revised: 18 December 2023

Accepted: 25 December 2023

Published: 27 December 2023



Copyright: © 2023 by the authors. Licensee MDPI, Basel, Switzerland. This article is an open access article distributed under the terms and conditions of the Creative Commons Attribution (CC BY) license (<https://creativecommons.org/licenses/by/4.0/>).

1. Introduction

The shortage of fossil fuels and increased global warming have created a demand for renewable energy sources. Thermoelectric materials, which directly convert waste heat or temperature gradient into electricity, have garnered a great deal of attention in recent years. Based on the range of temperature of operation, conventional thermoelectric materials are classified into three categories: (1) Bi_2Te_3 compounds with for $T < 150^\circ\text{C}$, (2) TAGS $[(\text{AgSbTe}_2)_{1-x}(\text{GeTe})_x]$ and PbTe-based compounds for $150^\circ\text{C} < T < 500^\circ\text{C}$, and (3) SiGe for $T > 500^\circ\text{C}$ [1]. Over time, half-Heusler alloys have also been investigated for their thermoelectric applications [2]. At the other end of the spectrum, Heusler alloys have also found wide applications in spintronics, a branch of nanoelectronics that relies on the spin of an electron rather than its charge. These devices operate on the principle of quantum tunneling and spin-transfer torque for MRAM applications [3]. Hence, Heusler alloys represent an important class of material for thermoelectric and spintronics applications.

Half-metallic ferromagnetic materials have attracted considerable attention in the last few years owing to their unique physical characteristics. These materials display a

metallic behavior near the Fermi energy surface in one spin channel and a semiconducting behavior near the Fermi energy level in the other spin channel, which yields a perfect spin polarization of 100% [4]. As a result, these materials could produce highly spin-polarized currents that could potentially improve the efficiency of spintronics devices. Numerous materials, for instance Heusler alloys, perovskites, and chalcogenides, have been reported to have a half-metallic behavior [5–8]. Several Heusler alloys (HAs) have been investigated theoretically for their half-metallicity and high Curie temperatures [9–11] that were further confirmed experimentally [12,13]. There are three groups of HAs that can be classified based on their chemical structures: full-Heusler alloys (FHAs), half-Heusler alloys (HHAs), and quaternary-Heusler alloys (QHAs). The FHAs have a space group of $Fm\bar{3}m$ with prototype structure, such as Cu_2MnAl , and four interpenetrating cubic lattices. The chemical formula of these alloys is X_2YZ , where X and Y correspond to transition metal atoms and Z refers to an s - p atom [14]. The structure of HHAs is similar to that of FHAs, except for a missing an X atom that leads to a $C1_b$ structure with an XYZ chemical formula and an $F\bar{4}3m$ space group [15]. The chemical formula of the QHAs is $XX'YZ$ with a Y -type structure (LiMgPdSb prototype structure) and a space group of $F\bar{4}3m$ (no. 216) [16,17]. The QHAs have applications in spin-dependent electronics, including spin filters, spin valves, and thermoelectric devices [18,19].

Several studies have indicated that QHAs possess significant thermoelectric properties, such as high transport coefficients (Seebeck coefficient and electrical conductivity), variable lattice thermal conductivity, and a good thermoelectric performance [20–24]. This leads to promising figure of merit (ZT) values where ZT is defined as follows [25]:

$$ZT = \frac{S^2\sigma T}{(\kappa_e + \kappa_L)}. \quad (1)$$

In this equation, S , σ , T , κ_e , and κ_L refer to the Seebeck coefficient, electrical conductivity, absolute temperature, electronic thermal conductivity, and lattice thermal conductivity, respectively. To obtain a high value of figure of merit ZT , alloys should have a high S and σ values, whereas κ_L should be as low as possible [26].

There are several studies on the subject of the thermoelectric properties of QHAs. For instance, Alqurashi and Hamad predicted ZT values of 1.13, 0.62, and 0.92 for VTiRhSi , VTiRhGe , and VTiRhSn alloys, respectively, at 800 K [24]. Previous computations predicted maximum S values of 44.3 and 53.44 $\mu\text{V}/\text{K}$ for CoRuMnAs and CoRhMnAs alloys, respectively [11]. Promising power factor values of 07.56×10^{-5} and $21.05 \times 10^{-5} \text{ Wm}^{-1}\text{K}^{-2}\text{s}^{-1}$ at 300 K were predicted for LaCoCrAl and LaCoCrGa QHAs, respectively [27]. Other calculations predicted ZT values of 0.61 and 0.71 for CoFeTiGe and CoFeCrGe , respectively [28]. Furthermore, the PdZrTiAl alloy was found to be a half-metallic ferromagnet with a 100% spin polarization and a 3 μ_B total magnetic moment [29]. Alqurashi et al. [30] predicted a similar half-metallic ferromagnetic behavior for VTiRhGa and VTiRhIn QHAs with a 100% spin polarization and a 3 μ_B total magnetic moment.

In this work, we report on ab initio investigations based on DFT to calculate the structural, dynamical, electronic, magnetic, and thermoelectric properties of novel CoMRhSi ($M = \text{Cr, Mn}$) quaternary Heusler alloys. To the best of our knowledge, this study investigates and reports the formation of these alloys along with spintronic and thermoelectric properties for the first time. The paper is organized as follows: in Section 2 the computational methodology is described, Section 3 presents the results and discussions, and Section 4 is devoted to the conclusions.

2. Computational Methodology

The structural optimization and energetic calculations are performed using the DFT method as implemented in VASP code [31]. The cut-off energy is selected to be 520 eV, while the total energy tolerance is 10^{-8} eV. The total energy calculations are performed using a $22 \times 22 \times 22$ k-mesh. The formation energy is calculated based on the results of the total energy. The phonon calculations using the Phonopy package are considered to investigate

the dynamical stability of the QHAs [32]. For these calculations, a supercell of $4 \times 4 \times 4$ is used with a $4 \times 4 \times 4$ k-mesh and cut-off energy of 500 eV. The supercell of QHAs unit-cell contains 256 atoms. The electronic and magnetic properties were computed within the full-potential linearized augmented plane wave (FP-LAPW) method as implemented in WIEN2k code [33]. The generalized gradient approximation (GGA) within Perdew–Burke–Ernzerhof (PBE) formalism was utilized to treat the exchange–correlation potential [34]. The $K_{\max} \times R_{\text{MT}}$ value was selected to be 9, where K_{\max} is the highest reciprocal lattice vector of the plane wave expansion and R_{MT} is the smallest atomic muffin tin radius. The R_{MT} values were selected as 2.3, 2.2, 2.1 and 1.8 atomic units (a.u.) for Co, M ($M = \text{Cr, Mn, Rh, and Si}$ atoms, respectively). The total energy and force tolerances were set to 10^{-4} Ry and 1 mRy/au, respectively. We adopted the VASP pseudopotential code for the structural optimization and WIEN2K full-potential code for the electronic and magnetic properties. For instance, in the case of structural optimization, VASP uses a smaller basis set which leads to faster calculations [35]; whereas, for electronic and magnetic properties, all electron calculations (WIEN2k) give more precise results [36].

The transport coefficients are considered by applying the Boltzmann transport theory as implemented in BoltzTraP code [37,38]. The S , σ , and κ_e parameters are estimated using the following equations [24,39]:

$$S_{\alpha\beta}(T, \mu) = \frac{1}{eT\Omega\sigma_{\alpha\beta}(T, \mu)} \int \bar{\sigma}_{\alpha\beta}(\varepsilon)(\varepsilon - \mu) \left[-\frac{\partial f_0(T, \varepsilon, \mu)}{\partial \varepsilon} \right] d\varepsilon \quad (2)$$

$$\sigma_{\alpha\beta}(T, \mu) = \frac{1}{\Omega} \int \bar{\sigma}_{\alpha\beta}(\varepsilon) \left[-\frac{\partial f_0(T, \varepsilon, \mu)}{\partial \varepsilon} \right] d\varepsilon \quad (3)$$

$$\kappa_{\alpha\beta}^0(T, \mu) = \frac{1}{e^2 T \Omega} \int \bar{\sigma}_{\alpha\beta}(\varepsilon)(\varepsilon - \mu)^2 \left[-\frac{\partial f_0(T, \varepsilon, \mu)}{\partial \varepsilon} \right] d\varepsilon \quad (4)$$

Here α and β are tensor indices; μ , Ω , and f_0 are the chemical potential, unit cell volume, and the Fermi–Dirac distribution function, respectively. The thermoelectric properties are calculated by using $36 \times 36 \times 36$ centered k-mesh. The σ and κ_e were computed within the constant relaxation time (τ) approximation, which was selected to be 0.5×10^{-15} s. This value was utilized for comparable structures for instance VTiRhZ ($Z = \text{Si, Sn, In}$) and FeRhCrZ ($Z = \text{Si, Ge}$) [24,40]. Slack’s formula was used to compute the lattice thermal conductivity (κ_l) as follows [41–43]:

$$\kappa_l = A \frac{\bar{M}\Theta_D^3 V^{1/3}}{\gamma^2 n^{2/3} T}, \quad (5)$$

where, $A = \frac{2.43 \times 10^{-6}}{1 - \frac{0.514}{\gamma} + \frac{0.228}{\gamma^2}}$, and \bar{M} , Θ_D , V , γ , n , and T are the average atomic mass, Debye temperature, volume per atom, Grüneisen parameter, number of atoms in the primitive unit cell, and temperature, respectively. The Θ_D and γ are estimated by calculating the elastic constants of CoMRhSi ($M = \text{Cr, Mn}$) QHAs. It is important to note that the Debye temperature can also be calculated from the vibrational density of states spectra, which could lead to a different value of Θ_D . However, there are reports as presented in reference [44] that the results of these two methods give a comparable output.

To compute the elastic constant, the IBRON was selected to be 6 in order to calculate the fourth-order elastic moduli tensor. The above IBRON number uses finite differences to calculate second derivatives of the Hessian matrix (second order derivative of energy with respect to atomic positions) by performing a total of six distortions to the crystal structure. The shear (G) and bulk (B) moduli were calculated based on the Voigt–Reuss–Hill approximations [45,46] that are defined as

Voigt average:

$$G_V = \frac{1}{5}[(C_{11} - C_{12}) + 3C_{44}], \text{ and } B_V = \frac{1}{3}(C_{11} + 2C_{12}), \quad (6)$$

Reuss average:

$$G_R = \frac{5C_{44}(C_{11} - C_{12})}{3(C_{11} - C_{12}) + 4C_{44}}, \text{ and } B_R = \frac{(C_{11} + C_{12})C_{11} - 2C_{12}^2}{3(C_{11} - C_{12})}, \quad (7)$$

Hill average:

$$G = \frac{1}{2}(G_V + G_R), \text{ and } B = \frac{1}{2}(B_V + B_R), \quad (8)$$

Using G and B from Equation (8), Young's modulus (E) and Poisson's ratio (ν) are calculated by [45,46] such that

$$E = \left(\frac{9BG}{3B + G} \right), \quad (9)$$

$$\nu = \left(\frac{3B - 2G}{2(3B + G)} \right), \quad (10)$$

Moreover, the Θ_D and (γ) are estimated as follows [45,46]:

$$\Theta_D = \frac{h}{k_B} \left(\frac{3n\rho N_A}{4\pi M} \right)^{1/3} v_m, \quad (11)$$

$$\gamma = \frac{9 - 12(v_t/v_l)^2}{2 + 4(v_t/v_l)^2}. \quad (12)$$

The parameters h , ρ , N_A , k_B , and M refer to the Planck constant, density, Avogadro's number, the Boltzmann constant, and the molecular weight, respectively. In addition, v_m , v_l and v_t are the average, transverse, and longitudinal sound velocities, which are given by [47,48] as follows:

$$v_t = \sqrt{\frac{G}{\rho}} \quad (13)$$

$$v_l = \sqrt{\frac{Y(1 - \nu)}{\rho(1 + \nu)(1 - 2\nu)}} \quad (14)$$

$$v_a = \left[\frac{1}{3} \left(\frac{2}{v_t^3} + \frac{1}{v_l^3} \right) \right]^{-\frac{1}{3}} \quad (15)$$

The lattice thermal conductivity (κ_l) values are computed by substituting Θ_D and γ values into Equation (5).

3. Results and Discussions

3.1. Structural Properties

The CoMRhSi ($M = \text{Cr, Mn}$) QHAs have a face-centered cubic LiMgPdSn (Y-type) configuration with (1:1:1) stoichiometry and a space group of $F\bar{4}3m$ (no. 216). Figure 1 illustrates the atomic configurations of these QHAs structures, Y-type-I, Y-type-II, and Y-type-III. The Wyckoff positions of the atoms in the three types are 4a (0,0,0), 4c (1/4, 1/4, 1/4), 4b (1/2, 1/2, 1/2), and 4d (3/4, 3/4, 3/4), see Table 1. The values of convex hull for both compounds, as predicted using OQMD, are -1.864 eV/f.u. for CoCrRhSi and -2.08 eV/f.u. for CoMnRhSi. The total energy calculations were performed for both QHAs in their three configuration types. These calculations predicted the Y-type-II configuration as the most stable structure of CoMRhSi ($M = \text{Cr, Mn}$) QHAs, see Table 2. These findings are consistent with prior calculations [49]. To determine if these QHAs can be synthesized experimentally and to confirm their thermodynamical stability, the formation enthalpy per formula unit is calculated using the following equation [50]:

$$E_{form} = E_{tot} - \left(E_{Co}^{bulk} + E_{Rh}^{bulk} + E_{Mn,Cr}^{bulk} + E_{Si}^{bulk} \right), \quad (16)$$

where E_{tot} is the equilibrium total energy per formula unit of the CoCrRhSi and CoMnRhSi alloys, and E_{Co}^{bulk} , E_{Rh}^{bulk} , E_Y^{bulk} , and $E_{Z=Si}^{bulk}$ are the total energies per atom in the bulk structure. In general, the negative value of the formation enthalpy indicates the feasibility of synthesizing the QHAs. The formation enthalpies of the CoCrRhSi and CoMnRhSi alloys are -1.32 and -1.91 eV/f.u., as shown in Table 3. These values agree with other previous calculations of similar structures such as CoNbMnSi (-1.74 eV/f.u.) and CoMoMnSi (-1.90 eV/f.u.) [48]. Moreover, the lattice parameters are found to be 5.78 Å and 5.83 Å for CoCrRhSi and CoMnRhSi as indicated in Table 3. These findings are in good agreement with the previously reported theoretical calculations [51,52].

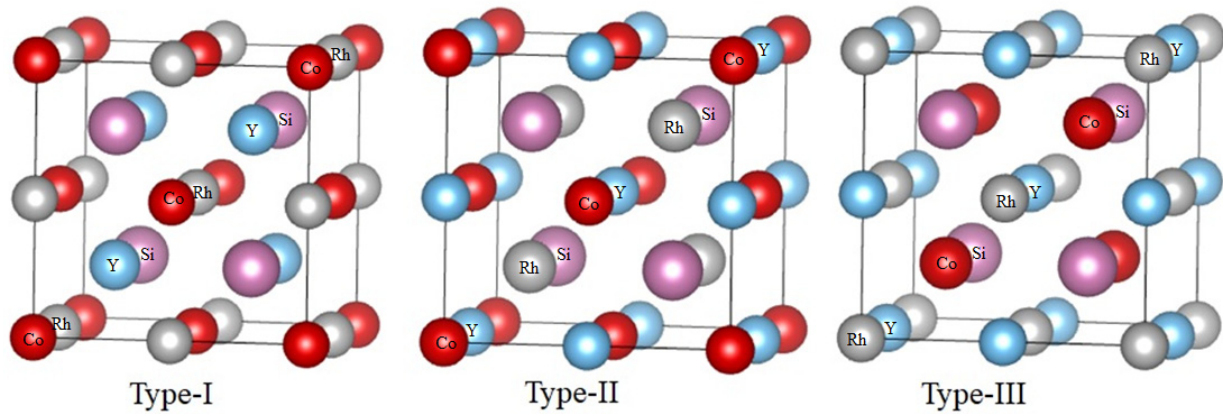


Figure 1. The three different types of the quaternary Heusler alloy primitive cells.

Table 1. The Wyckoff positions (4a, 4c, 4b, and 4d) of the elements in CoMRhSi ($M = Cr, Mn$) QHAs for three types of configurations.

Y	4a (0,0,0)	4b (1/2, 1/2, 1/2)	4c (1/4, 1/4, 1/4)	4d (3/4, 3/4, 3/4)
Type-I	Co	Rh	Y	Z
Type-II	Co	Y	Rh	Z
Type-III	Rh	Co	Y	Z

Table 2. The total energy in eV of CoMRhSi ($M = Cr, Mn$) QHAs in the three types of configurations.

Alloys	Type-I	Type-II	Type-III
CoCrRhSi	-29.719	-30.633	-30.145
CoMnRhSi	-29.187	-30.749	-29.918

Table 3. The formation energy E_{form} (eV/f.u.), lattice constant a (Å), elastic constants C_{ij} (GPa), bulk modulus B (GPa), Young's modulus E (GPa), isotropic shear modulus G (GPa), anisotropy factor A , Pugh's ratio B/G , Cauchy pressure C_p (GPa), anisotropy factor A , and the melting temperature T_{melt} (K) of CoMRhSi ($M = Mn, Cr$) QHAs.

Physical Parameter	CoCrRhSi	CoMnRhSi
E_{form}	-1.32	-1.91
a	5.78	5.83
C_{11}	335.89	334.40
C_{12}	145.23	141.94
C_{44}	58.91	72.14
B	216.88	211.45
E	185.23	216.13
G	68.35	81.29

Table 3. Cont.

Physical Parameter	CoCrRhSi	CoMnRhSi
B/G	3.17 3.39 ^{a)}	2.60
C_p	86.31	69.05
A	0.61	0.74
T_{melt}	2624	2574

^{a)} Ref [43].

3.2. Phonon Calculation

The analysis of the dynamical phonon properties of the CoMRhSi ($M = \text{Cr, Mn}$) alloys is presented here. The phonon dispersion curves (PDCs) provide information about the dynamical stability of the system. These phonon dispersion curves show only positive frequencies, indicating that both alloys are dynamically stable as indicated in Figure 2. The phonon dispersion curves of CoMRhSi ($M = \text{Mn, Cr}$) alloys exhibit twelve phonon branches since the primitive cell consists of four atoms. There are three acoustic phonon modes (one longitudinal (LA) and two transversal acoustic (TA)), and nine optical branches (three longitudinal (LO) and six transverse optical (TO)). These results are in good agreement with previous investigations on CoFeCrGe and CoFeTiGe QHAs [28].

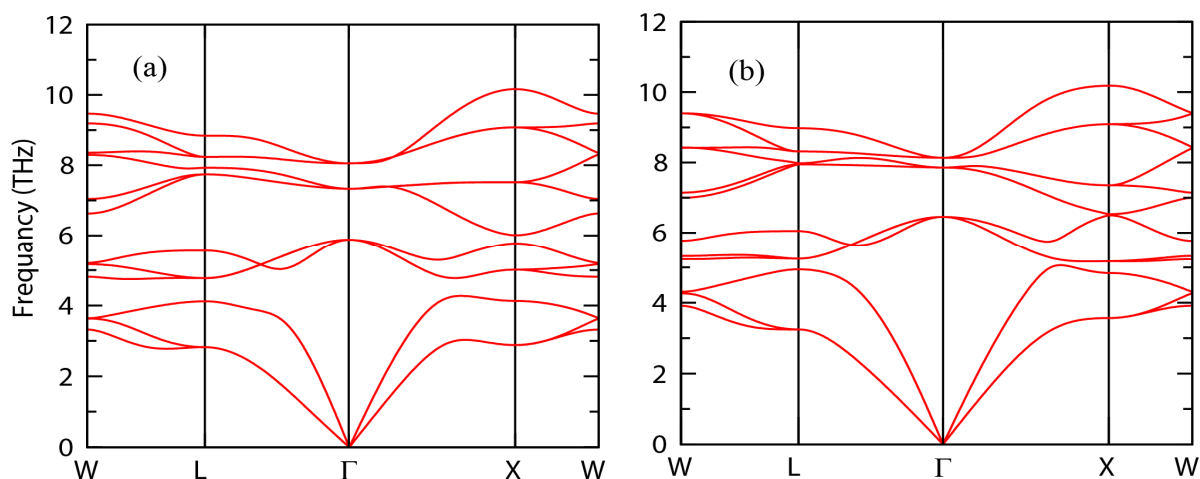


Figure 2. Phonon dispersion relation of (a) CoRhCrSi and (b) CoRhMnSi QHAs.

3.3. Mechanical Properties

The mechanical properties of CoMRhSi ($M = \text{Mn, Cr}$) alloys are presented by investigating the mechanical stability for the cubic configuration that is achieved by fulfilling the Born–Huang criteria [50] as follows:

$$C_{44} > 0, (C_{11} - C_{12}) > 0, (C_{11} + 2C_{12}) > 0, \text{ and } C_{12} < B < C_{11}, \quad (17)$$

where the three independent elastic constants (C_{11}), (C_{12}), and (C_{44}) are referred to longitudinal compression, transverse expansion, and the shear modulus predictor, and B refers to the Bulk modulus. The inequality conditions that are shown in Equation (17) are fulfilled for these alloys and thus the mechanical stability is confirmed. The results are summarized in Table 3. The B values were predicted to be 216.88 and 211.45 GPa for CoRhCrSi and CoRhMnSi alloys.

The three independent elastic constants were used to calculate the shear modulus (G), Young's modulus (E), Cauchy pressure (C_p), Poisson's ratio (ν), and the anisotropy factor (A). The results of these calculations are shown in Table 3. The above G , C_p , and A parameters are defined as follows [50–52]:

$$G = (G_V + G_R)/2 \quad (18)$$

$$C_p = C_{12} - C_{44} \quad (19)$$

$$A = 2C_{44}/(C_{11} - C_{12}) \quad (20)$$

G_R and G_V in Equation (18) are the shear moduli of Reuss, and Voigt. The E (G) values were calculated as 185.23 GPa (68.35 GPa) and 216.13 GPa (81.29 GPa) for CoRhCrSi and CoRhMnSi alloys. The large positive E and G values indicate that these alloys are rigid. These findings are consistent with prior predictions for CoCrScAl, CoCrScSi, CoCrScGe, and CoCrScGa alloys [53]. The Pugh's ratio (B/G) values of CoCrRhSi and CoMnRhSi alloys are 3.17 and 2.60, which are more than the standard value ($B/G > 1.75$ [54]). These results indicate that the alloys have a ductile nature behavior, and are in good agreement with prior calculations [28,50]. Moreover, the Cauchy pressure is calculated to explain the bonding of the alloys. If the Cauchy pressure is negative, the material is classified to have a covalent bonding. For metallic bonding, the Cauchy pressure is positive [50]. According to the present results, the C_p values of the CoCrRhSi and CoMnRhSi alloys were calculated as 86.31 and 69.05 GPa, which indicates a metallic bonding behavior for these alloys. In addition, the anisotropy factor, A , is calculated to test the anisotropy of the materials. If A values are different than unity, the materials are anisotropic [55]. The present calculation for A was found to be less than unity, which indicates the alloys are anisotropic materials. These results agree with previously reported calculations for ZrTiRhGe and ZrTiRhSn [56].

In order to provide an understanding of the heat resistance of the material, the melting point (T_{melt}) is calculated using the following formula [29,54,57]:

$$T_{melt} = \left[553 \text{ K} + \left(\frac{5.91 \text{ K}}{\text{GPa}} \right) C_{11} \right] \pm 300 \text{ K}. \quad (21)$$

This formula shows that the melting temperature depends on the longitudinal compression (C_{11}) of the alloys. As a result, the alloy with the larger longitudinal compression has a higher melting temperature. In this case, the CoCrRhSi alloy possesses a higher melting temperature as indicated in Table 3. The values of T_{melt} are found to be 2624 and 2547 K for CoCrRhSi and CoMnRhSi alloys, which are in good agreement with those obtained previously for CoFeCrGe (2584 K) and CoFeTiGe (2484 K) [28].

3.4. Electronic and Magnetic Properties

The band structure, total density of states (TDOS), and magnetic properties of CoMRhSi ($M = \text{Mn, Cr}$) QHAs are investigated as shown in Figure 3 for the CoMRhSi ($M = \text{Mn, Cr}$) alloys. The results presented in this figure show that the electronic bands of the majority spin channel overlap with the Fermi level, which indicates a metallic behavior. However, the minority spin channel shows a semiconducting behavior with an indirect band gap between the Γ and X high-symmetry points at the valence band maximum (VBM) and the conduction band minimum (CBM), respectively. The band gap values in the minority spin channels were found to be 0.54 eV and 0.57 eV for CoCrRhSi and CoMnRhSi. These results are in agreement with other calculations [48,56–61]. The spin polarization of QHAs can be determined using the following relationship [62,63]:

$$P = \frac{\rho_{\uparrow}(E_f) - \rho_{\downarrow}(E_f)}{\rho_{\uparrow}(E_f) + \rho_{\downarrow}(E_f)} \times 100, \quad (22)$$

where $\rho_{\uparrow}(E_f)$ and $\rho_{\downarrow}(E_f)$ are the majority and minority spin densities of states at the Fermi level (E_f). Thus, both the CoCrRhSi and CoMnRhSi alloys were found to have a 100% spin polarization due to the absence of the states at the minority spin channel. This is not the case for the majority spin channel, as indicated in Figure 3. The present results for the above alloys are in good agreement the results obtained for CoRhMnSi by Ghosh et al. [63]. This indicates that these alloys may demonstrate potential applications in spintronics.

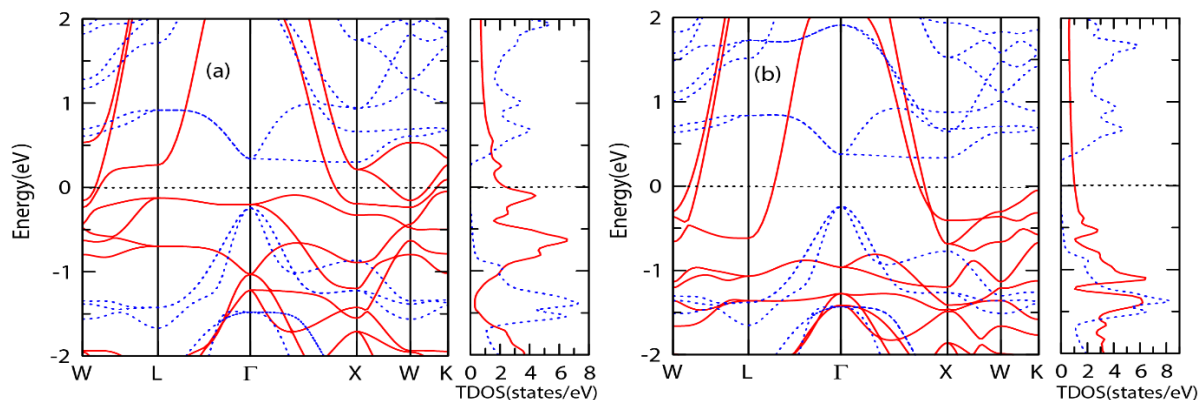


Figure 3. The electronic band structures and total density of states (TDOS) of (a) CoCrRhSi and (b) CoMnRhSi QHAs. The solid and dotted lines represent the majority and minority spin channels, respectively.

The magnetic structure of the QHAs was tested for three states: ferromagnetic, antiferromagnetic, and paramagnetic. The results show that the ferromagnetic state was found to be the most stable for these alloys. Table 4 presents the total and local magnetic moments of the CoMRhSi QHAs. Both the CoCrRhSi and CoMnRhSi alloys exhibit integer values of $4 \mu_B$ and $5 \mu_B$. A similar value of the net magnetic moment of $5 \mu_B$ for CoRhMnSi was obtained by Ghosh et al. [64]. These values are found to follow the Slater–Pauling rule for half-metallicity that is described as: $M_{tot} = (Z_{tot} - 24) \mu_B$, where M_{tot} and Z_{tot} refer to the total magnetic moment and the number of the total valence electrons. The significant contribution of the total magnetic moment of 2.41 and $3.31 \mu_B$ for the CoCrRhSi and CoMnRhSi alloys comes from the Cr and Mn atoms. The Co, Rh, and M ($M = \text{Cr}$, and Mn) atoms have a ferromagnetic coupling between their local magnetic moments in the two QHAs.

Table 4. The calculated band gap values E_g (eV), spin polarization P (%), total magnetic moment m_{total} (μ_B), local magnetic moments per atom m_i (μ_B) ($i = \text{Co, Cr, Mn Rh, Z}$) for the CoRhMSi ($M = \text{Cr, Mn}$) alloys.

Compound	E_g (eV)	P (%)	m_{Co} [μ_B]	m_{Rh} [μ_B]	m_Y [μ_B]	m_{Si} [μ_B]	m_{total} [μ_B]
CoCrRhSi	0.54 (minority)	100	1.15	0.36	2.41	−0.02	4.00 4.00 ^{a)}
CoMnRhSi	0.57 (minority)	100	1.25	0.44	3.31	−0.02	5.00

^{a)} Ref [43].

The linear relationship between the Curie temperature (T_C) and the total magnetic moment is one of the methods that can be used to calculate T_C as follows [65–67]:

$$T_C = 23 + 181M_{tot}, \quad (23)$$

where, M_{tot} is the total magnetic moment. Based on this equation, the T_C values of the CoCrRhSi and CoMnRhSi alloys are found to be 747 and 928 K, which means the ferromagnetic structure is retained for temperatures much higher than room temperature. However, it is important to note that this is just one of the methods to estimate the T_C and, very often, the results deviate from the experimental output. Hence, these values just serve as an estimate of the actual values of the transition temperature.

3.5. Transport Properties and ZT

The transport properties were calculated for the CoMRhSi ($M = \text{Mn, Cr}$) QHAs' stable structures. The calculations were performed using Boltzmann transport theory with a constant relaxation time approximation [38]. The total S and σ of the majority and minority spin channels are calculated by using the two-current model as [27]:

$$S = \frac{S_{\uparrow} \sigma_{\uparrow} + S_{\downarrow} \sigma_{\downarrow}}{\sigma_{\uparrow} + \sigma_{\downarrow}}. \quad (24)$$

Here S_{\uparrow} (S_{\downarrow}) and σ_{\uparrow} (σ_{\downarrow}) represent the Seebeck coefficient and electrical conductivity for the majority (minority) spin channels.

The results of the total Seebeck coefficient are shown in Figure 4a,b as a function of the chemical potential ($E-E_f$) at 300 and 800 K. The figure shows that the total S values of these alloys increase by increasing the temperature. The CoMnRhSi alloy has higher values of the total S than those of the CoCrRhSi alloy. The values of the total electrical conductivity (σ) as a function of ($E-E_f$) at 300 and 800 K are depicted in Figure 4c,d. As seen in the figures, the n-type doping level shows higher σ values than those of the p-type. Moreover, the temperature effect on σ values appear to be minimal. Figure 4e,f exhibit the power factor (PF) as a function of ($E-E_f$) at 300 and 800 K. The PF values are found to be higher as the temperature increases with maximum values of 20.2×10^{11} and 31.1×10^{11} ($\text{W/m K}^2 \text{s}$) for the CoCrRhSi and CoMnRhSi alloys at 800 K.

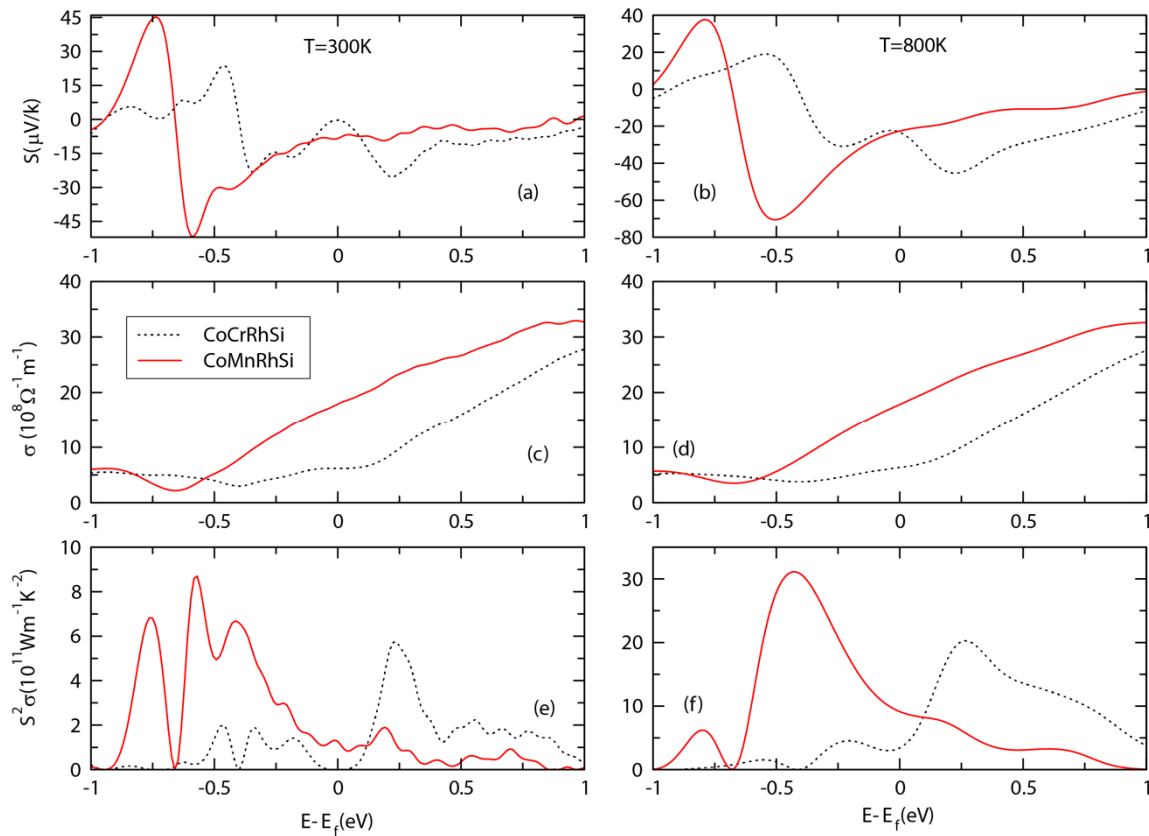


Figure 4. (a,b) The Seebeck coefficient (S), (c,d) electrical conductivity (σ), and (e,f) power factor ($S^2\sigma$) as a function of the chemical potential at temperatures of 300 K, 800 K for the CoRhMSi ($M = \text{Mn, Cr}$) QHAs.

Figure 5a,b present the electronic thermal conductivity (κ_e) of CoMRhSi ($M = \text{Mn, Cr}$) QHAs as a function of ($E-E_f$) at 300 and 800 K. From these figures, one can notice that the κ_e values of the CoMnRhSi alloy are higher than those of the CoCrRhSi alloy. The values of the

lattice thermal conductivity (κ_l) of CoMRhSi ($M = \text{Mn, Cr}$) QHAs are calculated based on the Slack equation. The computed parameters Θ_D , γ , v_m , v_t , and v_l are presented in Table 5. The Θ_D (γ) values of the CoCrRhSi and CoMnRhSi alloys are found to be 420.78 (2.19) and 454.28 K (1.97). These results are in good agreement with the previous calculation [46]. Figure 5c presents κ_l as a function of temperature. The κ_l values are found to be 1.10 and 0.69 W/m·K at 800 K for the CoCrRhSi and CoMnRhSi alloys, which are significantly low as compared to those of other QHAs such as CoFeCrGe (11.01 W/m·K and CoFeTiGe (12.26 W/m·K) [28]. Figure 6 show the figure of merit ZT values as a function of $(E-E_f)$ at 300 K and 800 K. The CoRhMSi ($M = \text{Mn, Cr}$) alloys have higher ZT values at 800 than those at 300 K. The highest ZT values at 800 K are the n-type 0.84 and the p-type 2.04 for CoCrRhSi and CoMnRhSi, respectively.

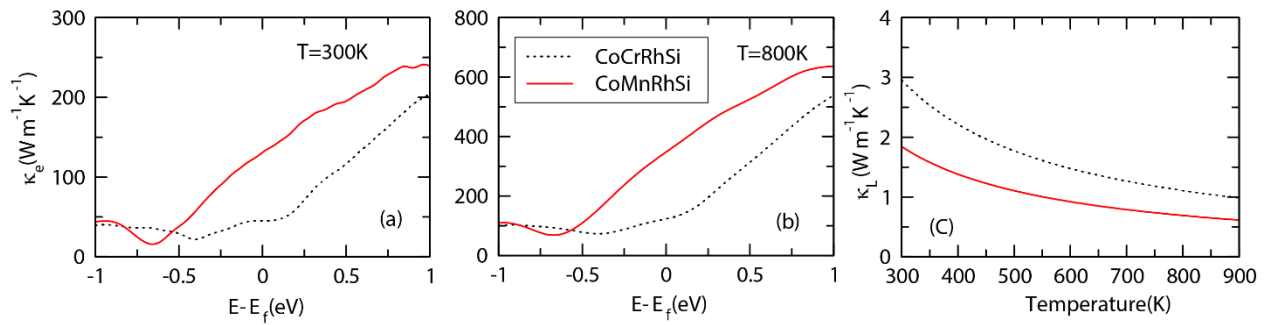


Figure 5. (a,b) The electronic thermal conductivity (κ_e) as a function of the temperature for CoRhMSi ($M = \text{Mn, Cr}$) as a function of the chemical potential at 300 K and 800 K, respectively. (c) The lattice thermal conductivity (κ_l) as a function of temperature for the CoRhMSi ($M = \text{Mn, Cr}$) alloys.

Table 5. The Debye temperature Θ_D (K), average sound velocity v_m (m/s), transverse sound velocity v_t (m/s), longitudinal sound velocity v_l (m/s), density ρ (kg/m³), and Grüneisen parameter γ for CoRhMSi ($M = \text{Mn, Cr}$) QHAs.

Alloys	Θ_D	v_m	v_t	v_l	ρ	γ
CoCrRhSi	420.78	3274.84	2909.84	6176.90	8186.08	2.19
CoMnRhSi	454.28	3533.46	3151.32	6250.75	8073.10	1.97

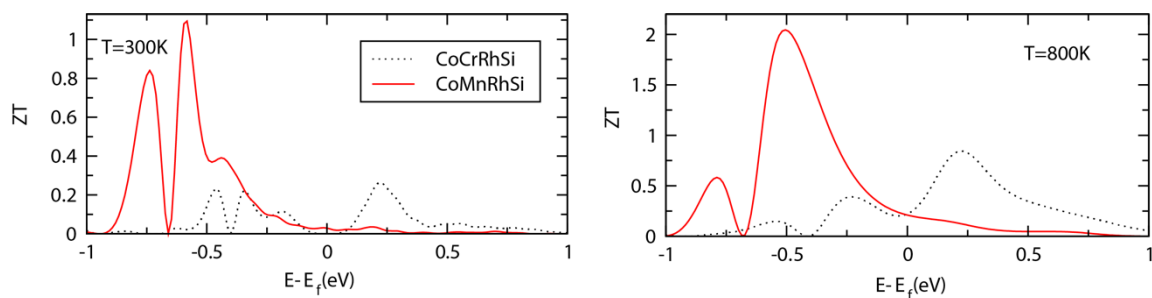


Figure 6. Calculated figure of merit (ZT) as a function of the chemical potential at (300 K, 800 K) for the CoRhMSi ($M = \text{Mn, Cr}$) alloys.

4. Conclusions

Density functional theory calculations were performed to investigate the structural, thermodynamic, dynamical, mechanical, electronic, magnetic, and thermoelectric properties of CoRhMSi ($M = \text{Mn, Cr}$) QHAs. Based on the total energy, phonon and elastic constant calculations, the Y-Type-II structure of CoRhMSi ($M = \text{Mn, Cr}$) QHAs was found to be the most stable configuration. Both CoCrRhSi and CoMnRhSi QHAs are predicted to be half-metallic with indirect band gaps of 0.542 and 0.576 eV in the minority spin channel, which yields a 100% spin polarization. The total magnetic moment of the CoCrRhSi and

CoMnRhSi alloys was found to be 4.00 and 5.00 μ_B . In addition, the Curie temperatures of the CoCrRhSi and CoMnRhSi alloys were calculated to be 747 and 928 K. The half metallicity and the ferromagnetic structure with Curie temperatures higher than the room temperatures of CoRhMSi ($M = \text{Mn, Cr}$) QHAs appear to be promising for spintronic applications.

The thermoelectric properties for CoMRhSi ($M = \text{Mn, Cr}$) QHAs were obtained using the semi-classical Boltzmann transport theory. The maximum power factor values for CoCrRhSi and CoMnRhSi QHAs at 800 K are 20.2×10^{11} and 31.1×10^{11} ($\text{W/m K}^2 \text{ s}$). The highest ZT values of the CoMnRhSi and CoCrRhSi alloys were also found to be 2.04 and 0.84 at 800 K. As a result, these alloys have the potential to be utilized in high-temperature thermoelectric applications.

Author Contributions: A.H.: validation, investigation, writing—original draft. H.A.: conceptualization, methodology, investigation, software, formal analysis, writing—review and editing. E.A.: investigation, writing—review and editing. B.H.: supervision, project administration, writing—review and editing. M.O.M.: writing—review and editing. All authors have read and agreed to the published version of the manuscript.

Funding: This research received no external funding.

Data Availability Statement: Data are contained within the article.

Acknowledgments: Abdullah Hzzazi and Hind Alqurashi were financially supported by the Saudi Arabian Cultural Mission. The calculations were performed at the high-performance computing center, University of Arkansas. This work is partially supported by the Open Access Publishing Fund administered through the University of Arkansas Libraries.

Conflicts of Interest: The authors declare that they have no conflicts of interest.

References

1. Zoui, M.A.; Bentouba, S.; Stocholm, J.G.; Bourouis, M. A Review on Thermoelectric Generators: Progress and Applications. *Energies* **2020**, *13*, 3606. [[CrossRef](#)]
2. Quinn, R.J.; Bos, J.-W.G. Advances in half-Heusler alloys for thermoelectric power generation. *Mater. Adv.* **2021**, *2*, 6246–6266. [[CrossRef](#)]
3. Peng, S.Z.; Zhang, Y.; Wang, M.X.; Zhang, Y.G.; Zhao, W. Magnetic Tunnel Junctions for Spintronics: Principles and Applications. In *Wiley Encyclopedia of Electrical and Electronics Engineering*; Wiley: Hoboken, NJ, USA, 2014; pp. 1–16. [[CrossRef](#)]
4. Oogane, M.; Sakuraba, Y.; Nakata, J.; Kubota, H.; Ando, Y.; Sakuma, A.; Miyazaki, T. Large tunnel magnetoresistance in magnetic tunnel junctions using Co₂MnX ($X \leq \text{Al, Si}$) Heusler alloys. *J. Phys. D Appl. Phys.* **2006**, *39*, 834–841. [[CrossRef](#)]
5. Xie, W.-H.; Liu, B.-G.; Pettifor, D.G. Half-metallic ferromagnetism in transition metal pnictides and chalcogenides with wurtzite structure. *Phys. Rev. B* **2003**, *68*, 134407. [[CrossRef](#)]
6. Khandy, S.A.; Gupta, D.C. Investigation of the transport, structural and mechanical properties of half-metallic REMnO₃ (RE = Ce and Pr) ferromagnets. *RSC Adv.* **2016**, *6*, 97641–97649. [[CrossRef](#)]
7. Mir, S.A.; Gupta, D.C. Understanding the origin of half-metallicity and thermophysical properties of ductile La₂CuMnO₆ double perovskite. *Int. J. Energy Res.* **2019**, *43*, 4783–4796. [[CrossRef](#)]
8. Şaşıoğlu, E.; Galanakis, I.; Sandratskii, L.M.; Bruno, P. Stability of ferromagnetism in the half-metallic pnictides and similar compounds: A first-principles study. *J. Phys. Condens. Matter* **2005**, *17*, 3915–3930. [[CrossRef](#)] [[PubMed](#)]
9. Graf, T.; Felser, C.; Parkin, S.S. Simple rules for the understanding of Heusler compounds. *Prog. Solid State Chem.* **2011**, *39*, 1–50. [[CrossRef](#)]
10. Wurmehl, S.; Fecher, G.H.; Kandpal, H.C.; Ksenofontov, V.; Felser, C.; Lin, H.J.; Morais, J. Geometric, electronic, and magnetic structure of Co₂FeSi: Curie temperature and magnetic moment measurements and calculations. *Phys. Rev. B Condens. Matter Mater. Phys.* **2005**, *72*, 184434. [[CrossRef](#)]
11. Alsayegh, S.; Alqurashi, H.; Andharah, E.; Hamad, B.; Manasreh, M. First-principal investigations of the electronic, magnetic, and thermoelectric properties of CrTiRhAl quaternary Heusler alloy. *J. Magn. Magn. Mater.* **2023**, *568*, 170421. [[CrossRef](#)]
12. Ishida, S.; Masaki, T.; Fujii, S.; Asano, S. Theoretical search for half-metallic films of Co₂MnZ (Z = Si, Ge). *Phys. B Condens. Matter* **1998**, *245*, 1–8. [[CrossRef](#)]
13. Sakuraba, Y.; Nakata, J.; Oogane, M.; Kubota, H.; Ando, Y.; Sakuma, A.; Miyazaki, T. Huge spin-polarization of L21-ordered Co₂MnSi epitaxial heusler alloy film. *Jpn. J. Appl. Phys. Part 2 Lett.* **2005**, *44*, L1100. [[CrossRef](#)]
14. Seh, A.Q.; Gupta, D.C. Exploration of highly correlated Co-based quaternary Heusler alloys for spintronics and thermoelectric applications. *Int. J. Energy Res.* **2019**, *43*, 8864–8877. [[CrossRef](#)]
15. Haleoot, R.; Hamad, B. Ab Initio Investigations of the Structural, Electronic, Magnetic, and Thermoelectric Properties of CoFeCuZ (Z = Al, As, Ga, In, Pb, Sb, Si, Sn) Quaternary Heusler Alloys. *J. Electron. Mater.* **2019**, *48*, 1164–1173. [[CrossRef](#)]

16. Bainsla, L.; Suresh, K.G. Equiatomic quaternary Heusler alloys: A material perspective for spintronic applications. *Appl. Phys. Rev.* **2016**, *3*, 031101. [[CrossRef](#)]
17. Andharia, E.; Alqurashi, H.; Hamad, B. Lattice Dynamics, Mechanical Properties, Electronic Structure and Magnetic Properties of Equiatomic Quaternary Heusler Alloys CrTiCoZ (Z = Al, Si) Using First Principles Calculations. *Materials* **2022**, *15*, 3128. [[CrossRef](#)] [[PubMed](#)]
18. Yousuf, S.; Gupta, D.C. Thermoelectric and mechanical properties of gapless Zr₂MnAl compound. *Indian J. Phys.* **2017**, *91*, 33–41. [[CrossRef](#)]
19. Takahashi, Y.K.; Kasai, S.; Hirayama, S.; Mitani, S.; Hono, K. All-metallic lateral spin valves using Co₂Fe(Ge_{0.5}Ga_{0.5}) Heusler alloy with a large spin signal. *Appl. Phys. Lett.* **2012**, *100*, 052405. [[CrossRef](#)]
20. Zhang, L.; Cheng, Z.X.; Wang, X.T.; Khenata, R.; Rozale, H. First-Principles Investigation of Equiatomic Quaternary Heusler Alloys NbVMnAl and NbFeCrAl and a Discussion of the Generalized Electron-Filling Rule. *J. Supercond. Nov. Magn.* **2018**, *31*, 189–196. [[CrossRef](#)]
21. Eliassen, S.N.H.; Katre, A.; Madsen, G.K.H.; Persson, C.; Løvvik, O.M.; Berland, K. Lattice thermal conductivity of Ti_xZr_yHf_{1-x-y}NiSn half-Heusler alloys calculated from first principles: Key role of nature of phonon modes. *Phys. Rev. B* **2017**, *95*, 045202. [[CrossRef](#)]
22. Lue, C.S.; Chen, C.F.; Lin, J.Y.; Yu, Y.T.; Kuo, Y.K. Thermoelectric properties of quaternary Heusler alloys Fe₂VA_{1-x}Si_x. *Phys. Rev. B Condens. Matter Mater. Phys.* **2007**, *75*, 064204. [[CrossRef](#)]
23. Yabuuchi, S.; Okamoto, M.; Nishide, A.; Kurosaki, Y.; Hayakawa, J. Large Seebeck Coefficients of Fe₂TiSn and Fe₂TiSi: First-Principles Study. *Appl. Phys. Express* **2013**, *6*, 025504. [[CrossRef](#)]
24. Alqurashi, H.; Hamad, B. Magnetic structure, mechanical stability and thermoelectric properties of VTiRhZ (Z = Si, Ge, Sn) quaternary Heusler alloys: First-principles calculations. *Appl. Phys. A Mater. Sci. Process.* **2021**, *127*, 1–11. [[CrossRef](#)]
25. Alqurashi, H.; Haleoot, R.; Pandit, A.; Hamad, B. Investigations of the electronic, dynamical, and thermoelectric properties of Cd_{1-x}Zn_xO alloys: First-principles calculations. *Mater. Today Commun.* **2021**, *28*, 102511. [[CrossRef](#)]
26. Kraemer, D.; Poudel, B.; Feng, H.-P.; Caylor, J.C.; Yu, B.; Yan, X.; Ma, Y.; Wang, X.; Wang, D.; Muto, A.; et al. High-performance flat-panel solar thermoelectric generators with high thermal concentration. *Nat. Mater.* **2011**, *10*, 532–538. [[CrossRef](#)] [[PubMed](#)]
27. Singh, S.; Gupta, D.C. Lanthanum based quaternary Heusler alloys LaCoCrX (X = Al, Ga): Hunt for half-metallicity and high thermoelectric efficiency. *Results Phys.* **2019**, *13*, 102300. [[CrossRef](#)]
28. Haleoot, R.; Hamad, B. Thermodynamic and thermoelectric properties of CoFeYGe (Y = Ti, Cr) quaternary Heusler alloys: First principle calculations. *J. Phys. Condens. Matter* **2019**, *32*, 075402. [[CrossRef](#)] [[PubMed](#)]
29. Ilkhani, M.; Boochani, A.; Amiri, M.; Asshabi, M.; Rai, D.P. Mechanical stability and thermoelectric properties of the PdZrTiAl quaternary Heusler: A DFT study. *Solid State Commun.* **2020**, *308*, 113838. [[CrossRef](#)]
30. Alqurashi, H.; Haleoot, R.; Hamad, B. First-principles investigations of the electronic, magnetic and thermoelectric properties of VTiRhZ (Z = Al, Ga, In) Quaternary Heusler alloys. *Mater. Chem. Phys.* **2021**, *278*, 125685. [[CrossRef](#)]
31. Kresse, G.; Joubert, D. From ultrasoft pseudopotentials to the projector augmented-wave method. *Phys. Rev. B* **1999**, *59*, 1758–1775. [[CrossRef](#)]
32. Kresse, G.; Hafner, J. *Ab initio* molecular dynamics for liquid metals. *Phys. Rev. B* **1993**, *47*, 558–561. [[CrossRef](#)] [[PubMed](#)]
33. Blaha, P.; Schwarz, K.; Sorantin, P.; Trickey, S. Full-potential, linearized augmented plane wave programs for crystalline systems. *Comput. Phys. Commun.* **1990**, *59*, 399–415. [[CrossRef](#)]
34. Perdew, J.P.; Burke, K.; Ernzerhof, M. Generalized gradient approximation made simple. *Phys. Rev. Lett.* **1996**, *77*, 3865–3868. [[CrossRef](#)] [[PubMed](#)]
35. Probert, M.I.J.; Hasnip, P.J.; Lejaeghere, K.; Bihlmayer, G.; Bjorkman, T.; Blaha, P.; Blum, V.; Caliste, D.; Castelli, I.E.; Dal Corso, A.; et al. Reproducibility in density functional theory calculations of solids. *Science* **2016**, *351*, 1415. [[CrossRef](#)]
36. Kishore, M.R.A.; Okamoto, H.; Patra, L.; Vidya, R.; Sjästad, A.O.; Fjellvåg, H.; Ravindran, P. Theoretical and experimental investigation on structural, electronic and magnetic properties of layered Mn₅O₈. *Phys. Chem. Chem. Phys.* **2016**, *18*, 27885–27896. [[CrossRef](#)] [[PubMed](#)]
37. Madsen, G.K.; Carrete, J.; Verstraete, M.J. BoltzTraP2, a program for interpolating band structures and calculating semi-classical transport coefficients. *Comput. Phys. Commun.* **2018**, *231*, 140–145. [[CrossRef](#)]
38. Madsen, G.K.; Singh, D.J. BoltzTraP. A code for calculating band-structure dependent quantities. *Comput. Phys. Commun.* **2006**, *175*, 67–71. [[CrossRef](#)]
39. Lin, T.; Gao, Q.; Liu, G.; Dai, X.; Zhang, X.; Zhang, H. Dynamical stability, electronic and thermoelectric properties of quaternary ZnFeTiSi Heusler compound. *Curr. Appl. Phys.* **2019**, *19*, 721–727. [[CrossRef](#)]
40. Khandy, S.A.; Chai, J.-D. Thermoelectric properties, phonon, and mechanical stability of new half-metallic quaternary Heusler alloys: FeRhCrZ (Z = Si and Ge). *J. Appl. Phys.* **2020**, *127*, 165102. [[CrossRef](#)]
41. Hong, A.J.; Li, L.; He, R.; Gong, J.J.; Yan, Z.B.; Wang, K.F.; Liu, J.M.; Ren, Z.F. Full-scale computation for all the thermoelectric property parameters of half-Heusler compounds. *Sci. Rep.* **2016**, *6*, 22778. [[CrossRef](#)]
42. Ma, H.; Yang, C.-L.; Wang, M.-S.; Ma, X.-G.; Yi, Y.-G. Effect of M elements (M = Ti, Zr, and Hf) on thermoelectric performance of the half-Heusler compounds MCoBi. *J. Phys. D Appl. Phys.* **2019**, *52*, 25550. [[CrossRef](#)]
43. Slack, G. Nonmetallic crystals with high thermal conductivity. *J. Phys. Chem. Solids* **1973**, *34*, 321–335. [[CrossRef](#)]

44. Chen, Q.; Sundman, B. Calculation of debye temperature for crystalline structures—A case study on Ti, Zr, and Hf. *Acta Mater.* **2001**, *49*, 947–961. [[CrossRef](#)]
45. Hill, R. The Elastic Behaviour of a Crystalline Aggregate. *Proc. Phys. Soc. Sect. A* **1952**, *65*, 349. [[CrossRef](#)]
46. Horner, H. Lattice dynamics of quantum crystals. *Z. Phys.* **1967**, *205*, 72–89. [[CrossRef](#)]
47. Anderson, O.L. A simplified method for calculating the debye temperature from elastic constants. *J. Phys. Chem. Solids* **1963**, *24*, 909–917. [[CrossRef](#)]
48. Xiong, X.; Wan, R.; Zhang, Z.; Lei, Y.; Tian, G. First-principle investigation on the thermoelectric properties of XCoGe (X = V, Nb, and Ta) half-Heusler compounds. *Mater. Sci. Semicond. Process.* **2022**, *140*, 106387. [[CrossRef](#)]
49. Hoat, D.; Hoang, D.-Q.; Binh, N.T.; Naseri, M.; Rivas-Silva, J.; Kartamyshev, A.; Cocolletzi, G.H. First principles analysis of the half-metallic ferromagnetism, elastic and thermodynamic properties of equiatomic quaternary Heusler compound CoCrRhSi. *Mater. Chem. Phys.* **2021**, *257*, 123695. [[CrossRef](#)]
50. Kundu, A.; Ghosh, S.; Banerjee, R.; Ghosh, S.; Sanyal, B. New quaternary half-metallic ferromagnets with large Curie temperatures. *Sci. Rep.* **2017**, *7*, 1803. [[CrossRef](#)]
51. Zhao, J.-S.; Gao, Q.; Li, L.; Xie, H.-H.; Hu, X.-R.; Xu, C.-L.; Deng, J.-B. First-principles study of the structure, electronic, magnetic and elastic properties of half-Heusler compounds LiXGe (X = Ca, Sr and Ba). *Intermetallics* **2017**, *89*, 65–73. [[CrossRef](#)]
52. Wang, X.; Cheng, Z.; Wang, J.; Liu, G. A full spectrum of spintronic properties demonstrated by a C1_b-type Heusler compound Mn₂Sn subjected to strain engineering. *J. Mater. Chem. C* **2016**, *4*, 8535–8544. [[CrossRef](#)]
53. Berri, S. Computational Study of Structural, Electronic, Elastic, Half-Metallic and Thermoelectric Properties of CoCrScZ (Z = Al, Si, Ge, and Ga) Quaternary Heusler Alloys. *J. Supercond. Nov. Magn.* **2020**, *33*, 3809–3818. [[CrossRef](#)]
54. Chen, X.-R.; Zhong, M.-M.; Feng, Y.; Zhou, Y.; Yuan, H.-K.; Chen, H. Structural, electronic, elastic, and thermodynamic properties of the spin-gapless semiconducting Mn₂CoAl inverse Heusler alloy under pressure. *Phys. Status Solidi (b)* **2015**, *252*, 2830–2839. [[CrossRef](#)]
55. Semari, F.; Boulechfar, R.; Dahmane, F.; Abdiche, A.; Ahmed, R.; Naqib, S.; Bouhemadou, A.; Khenata, R.; Wang, X. Phase stability, mechanical, electronic and thermodynamic properties of the Ga₃Sc compound: An ab-initio study. *Inorg. Chem. Commun.* **2020**, *122*, 108304. [[CrossRef](#)]
56. Alqurashi, H.; Haleoot, R.; Hamad, B. First-principles investigations of Zr-based quaternary Heusler alloys for spintronic and thermoelectric applications. *Comput. Mater. Sci.* **2022**, *210*, 111477. [[CrossRef](#)]
57. Rached, H. Prediction of a new quaternary Heusler alloy within a good electrical response at high temperature for spintronics applications: DFT calculations. *Int. J. Quantum Chem.* **2021**, *121*, e26647. [[CrossRef](#)]
58. Benkabou, M.; Rached, H.; Abdellaoui, A.; Rached, D.; Khenata, R.; Elahmar, M.; Abidri, B.; Benkhattou, N.; Bin-Omran, S. Electronic structure and magnetic properties of quaternary Heusler alloys CoRhMnZ (Z = Al, Ga, Ge and Si) via first-principle calculations. *J. Alloys Compd.* **2015**, *647*, 276–286. [[CrossRef](#)]
59. Dag, T.S.; Gencer, A.; Ciftci, Y.; Surucu, G. Equiatomic quaternary CoXCraI (X = V, Nb, and Ta) Heusler compounds: Insights from DFT calculations. *J. Magn. Magn. Mater.* **2022**, *560*, 169620. [[CrossRef](#)]
60. Elahmar, M.; Rached, H.; Rached, D.; Benalia, S.; Khenata, R.; Biskri, Z.; Bin Omran, S. Structural stability, electronic structure and magnetic properties of the new hypothetical half-metallic ferromagnetic full-Heusler alloy CoNiMnSi. *Mater. Sci.* **2016**, *34*, 85–93. [[CrossRef](#)]
61. Gencer, A.; Surucu, O.; Usanmaz, D.; Khenata, R.; Candan, A.; Surucu, G. Equiatomic quaternary Heusler compounds TiVFeZ (Z = Al, Si, Ge): Half-metallic ferromagnetic materials. *J. Alloys Compd.* **2021**, *883*, 160869. [[CrossRef](#)]
62. Rached, H.; Rached, D.; Khenata, R.; Abidri, B.; Rabah, M.; Benkhattou, N.; Omran, S.B. A first principle study of phase stability, electronic structure and magnetic properties for Co_{2-x}Cr_xMnAl Heusler alloys. *J. Mag. Mag. Mater.* **2015**, *379*, 84. [[CrossRef](#)]
63. Bourachid, I.; Rached, D.; Rached, H.; Bentouaf, A.; Rached, Y.; Caid, M.; Abidri, B. Magneto-electronic and thermoelectric properties of V-based Heusler in ferrimagnetic phase. *Appl. Phys. A* **2022**, *128*, 493. [[CrossRef](#)]
64. Ghosh, S.; Ghosh, S. Site dependent substitution and half-metallic behaviour in Heusler compounds: A case study for Mn₂RhSi, Co₂RhSi and CoRhMnSi. *Comput. Condens. Matter.* **2019**, *21*, e00423. [[CrossRef](#)]
65. Candan, A.; Uğur, G.; Charifi, Z.; Baaziz, H.; Ellialtıoğlu, M. Electronic structure and vibrational properties in cobalt-based full-Heusler compounds: A first principle study of Co₂MnX (X = Si, Ge, Al, Ga). *J. Alloys Compd.* **2013**, *560*, 215–222. [[CrossRef](#)]
66. Elahmar, M.; Rached, H.; Rached, D.; Khenata, R.; Murtaza, G.; Bin Omran, S.; Ahmed, W. Structural, mechanical, electronic and magnetic properties of a new series of quaternary Heusler alloys CoFeMnZ (Z = Si, As, Sb): A first-principle study. *J. Magn. Magn. Mater.* **2015**, *393*, 165–174. [[CrossRef](#)]
67. Jain, R.; Jain, V.K.; Chandra, A.R.; Jain, V.; Lakshmi, N. Study of the Electronic Structure, Magnetic and Elastic Properties and Half-Metallic Stability on Variation of Lattice Constants for CoFeCrZ (Z = P, As, Sb) Heusler Alloys. *J. Supercond. Nov. Magn.* **2018**, *31*, 2399–2409. [[CrossRef](#)]

Disclaimer/Publisher’s Note: The statements, opinions and data contained in all publications are solely those of the individual author(s) and contributor(s) and not of MDPI and/or the editor(s). MDPI and/or the editor(s) disclaim responsibility for any injury to people or property resulting from any ideas, methods, instructions or products referred to in the content.